Journal of Magnetism and Magnetic Materials 380 (2015) 98–104

Contents lists available at ScienceDirect

Journal of Magnetism and Magnetic Materials

journal homepage: www.elsevier.com/locate/jmmm

Relating Mason number to Bingham number in magnetorheological fluids

Stephen G. Sherman, Andrew C. Becnel, Norman M. Wereley*

Department of Aerospace Engineering, University of Maryland, College Park, MD 20742, USA

ARTICLE INFO

Article history:
Received 30 June 2014
Received in revised form
31 October 2014
Accepted 2 November 2014
Available online 7 November 2014

Keywords:
Bingham number
Mason number
Magnetorheological fluid
Apparent viscosity

ABSTRACT

Magnetorheological (MR) fluids are described using two nondimensional numbers, the Bingham and Mason numbers. The Mason number is the ratio of particle magnetic forces to viscous forces and describes the behavior of MR fluids at the microscopic, particle level scale. At the macroscopic, continuum scale, Bingham number is the ratio of yield stress to viscous stress, and describes the bulk motion of the fluid. If these two nondimensional numbers can be related, then microscopic models can be directly compared to macroscopic results. We show that if microscopic and macroscopic forces are linearly related, then Bingham and Mason number are inversely related, or, alternatively, that the product of the Bingham number and the Mason number is a constant. This relationship is experimentally validated based on measurements of apparent viscosity on a high shear rate, $\dot{\gamma} \approx 10\,000\ s^{-1}$, Searle cell rheometer. This relationship between Mason number and Bingham number is then used to analyze a Mason number based result, and is also used to inform the MR fluid device design process.

1. Introduction

Magnetorheological (MR) fluid is a fluid composed of micron scale magnetizable particles suspended in a carrier fluid. Upon the application of field, the particles in the fluid align to form chain like structures, and these chains cause the fluid to develop a field dependent yield stress. The primary application of MR fluid has been in MR dampers and MR energy absorbers, where the controllable apparent viscosity allows for a controllable damping force or stroking load, which enables high performance vibration isolation [1] or shock mitigation that can adapt to payload weight and impact severity [2,3].

Models of magnetorheological fluids have typically taken two perspectives: either modeling the MR fluid as a collection of microscopic particles floating in a carrier fluid, or as a bulk fluid continuum. Microscopic modeling of MR fluids focuses on the behavior of the particles [4–6] by examining the formation and destruction of chain structures in the fluid with the goal of predicting yield stress. The primary forces on the particles that govern chain formation are viscous drag of the carrier fluid on the particle and the interparticle magnetic forces. The ratio of particle magnetic forces to viscous forces is known as the Mason number, Mn, [7–9], named after the work of Mason et. al. on the behavior of fluid droplets in the presence of electric field [10]. In the equations of motion, the Mason number is the governing parameter of the shear response of a particle in an MR fluid, and is an essential part of research on dynamic models of chain formation. The Mason number, Mn, also has value in the analysis of experimental data, such as when apparent viscosity is plotted against Mason number, the apparent viscosity curves collapse to a single curve, thereby reducing the dimensionality of a dataset [7,8].

At the bulk scale, one of the idealized descriptions of MR fluids is as a Bingham plastic [11], in which the applied magnetic field additively induces a field controllable yield stress to a Newtonian fluid. The Bingham number, Bi, which is the ratio of yield stress to viscous stress, describes the extent to which the controllable yield stress can exceed the viscous stress (typically $\mathrm{Bi} \gg 1$), and is an essential descriptor of Bingham plastic behavior. The Bingham number can be used to calculate flow rates, flow profiles, and pressure losses in devices using Bingham plastic fluids [12]. In particular, for shear mode MR devices, the Bingham number represents the controllable force ratio [13], and since MR fluids are used for the purpose of generating controllable forces, the Bingham number is an essential and fundamental parameter for the understanding and analysis of MR fluids at the bulk scale.

We seek to relate the Bingham number to the Mason number, two nondimensional numbers that represent fundamental descriptions of the behavior of MR fluid at macroscopic and microscopic scales respectively. In particular, we focus on MR fluids typically used in energy absorbing devices. These MR fluids are typically suspensions of 1–10 μm diameter carbonyl iron particles with solids loading ranging from 20 to 50 volume percent, and

* Corresponding author.
E-mail address: wereley@umd.edu (N.M. Wereley).

http://dx.doi.org/10.1016/j.jmmm.2014.11.010
0304-8853/

well described by the Bingham plastic model. By mathematically relating Bingham number to Mason number, we enable microscopic Mason number based analyses to be directly extended to macroscopic or device scale Bingham number based problems. Alternatively, experimental Bingham number based results can be scaled down for comparison to Mason number based particle level analyses.

In this study, the Bingham number and the Mason number are developed, and it is shown that if microscopic forces map linearly to macroscopic forces, then the Bingham number and the Mason number are inversely related, or that the product of Bingham number and Mason number is a constant. This notion is confirmed through measurements of apparent viscosity. We experimentally validate the claim that microscopic and macroscopic forces are linearly related, and that this is akin to assuming that MR fluids are well described by the Bingham plastic model. Finally, the relationship between Mason number and Bingham number is used to examine the experimental relevance of a Mason number based result, as well as how such a relationship would inform the MR fluid and/or device design process.

2. Background

To motivate the usage of these nondimensional numbers, both numbers are derived in the analytical context in which they arise.

2.1. The Bingham number

For device scale analyses, the fluid is treated as a continuum with nonlinear rheological properties. A typical MR fluid shear stress vs. shear rate graph is shown in Fig. 1. These shear stresses for each field strength are typically modeled by the Bingham plastic model,

$$\tau = \tau_y + \eta_{pl}\dot{\gamma}, \tag{1}$$

which has a plastic viscosity, η_{pl}, and a yield stress, τ_y. The yield stress is magnetic field dependent, and it is typical to assume that η_{pl} is independent of field strength, and equivalent to the off-state viscosity, η_{off}. In MR fluids, η_{pl} is chosen to be the slope of the high shear rate asymptote of the shear stress curve, and τ_y corresponds to the intersection of the high shear rate asymptote with the stress axis at $\dot{\gamma} = 0$.

A typical way in which MR fluid is used in damper design is the shear mode damper [13], where an upper plate moving with velocity, v, and area, A, moves over a stationary lower plate with a gap of d between the two plates. Here, the fluid velocity profile is linear, and the force on the upper plate is

$$F_d = \left(\tau_y + \eta_{pl}\frac{v}{d}\right)A. \tag{2}$$

The force in conventional viscous dampers can be written in the form $F_d = c_0 v$, where c_0 is the damping, and for a Newtonian fluid in shear mode $c_0 = \eta A/d$. For the shear mode MR damper, rearranging into this form yields

$$F_d = \left(\frac{\tau_y d}{\eta_{pl} v} + 1\right)\eta_{pl}\frac{A}{d}v = c_{eq}v, \tag{3}$$

where c_{eq} is the equivalent damping for a fluid with a yield stress. The ratio of equivalent damping to Newtonian damping yields the damping coefficient

$$\frac{c_{eq}}{c_0} = 1 + \frac{\tau_y d}{\eta_{pl} v} = 1 + \mathrm{Bi} \tag{4}$$

which describes the effect that the addition of a yield stress has on damping force. For an MR fluid, where the yield stress is field controllable, this ratio is the controllable force ratio. The term that governs controllability is the Bingham number,

$$\mathrm{Bi} = \frac{\tau_y}{\eta_{pl}\dot{\gamma}_c}, \tag{5}$$

the ratio of magnetic forces (τ_y) to viscous forces $\left(\eta_{pl}\dot{\gamma}_c\right)$ in the fluid, where $\dot{\gamma}_c$ is the characteristic shear rate of the system, which for a shear mode damper is $\dot{\gamma}_c = v/d$. Since the purpose of MR fluids is to generate a field controllable force, and the Bingham number represents the controllable force ratio of an MR device, it is clear that Bingham number is a fundamental representation of the behavior of MR fluids. In more complicated geometries, such as in pipe flow, the Bingham number becomes an essential intermediate quantity in the determination of the flow rate, flow profile, and controllable force output of an MR fluid device [12]. But at the fluid level, the Bingham number is a descriptive, empirical quantity, and does not tell us anything about what causes the MR effect, or how a fluid can be modified to improve its performance.

2.2. Mason number

Modeling MR fluid at the particle level allows us to develop predictive models of fluid behavior, providing insight into the chain formation that underlies the MR effect. At the microscopic scale, MR fluids consist of magnetizable particles suspended in a carrier fluid under the influence of an applied magnetic field, H_0. Fig. 2 contains a diagram of two interacting particles under shear and applied magnetic field. Typically, these are spherical carbonyl iron particles with diameter $\sigma = 1 - 10\,\mu\mathrm{m}$. The particles are

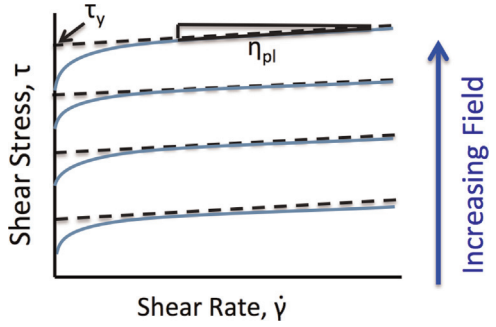

Fig. 1. Idealized rheogram or shear stress vs. shear rate diagram for an MR fluid.

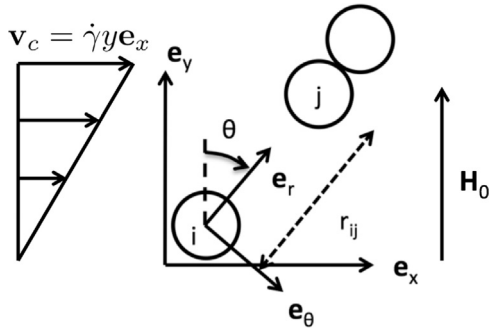

Fig. 2. Diagram of two particles in a shearing fluid.

usually modeled as perfect spheres with fixed point dipole moments m_i aligned with the applied field, $\mathbf{m}_i = \pi\sigma^3\mathbf{M}_p/6$, where magnetization, $\mathbf{M}_p = \chi_p\mathbf{H}_0$ is also aligned with the applied field. The force on particle i from particle j is

$$\mathbf{F}_{ij} = \frac{F_0}{(r_{ij}/\sigma)^4}\left[(3\cos^2\theta_{ij} - 1)\mathbf{e}_r + \sin 2\theta_{ij}\mathbf{e}_\theta\right] \tag{6}$$

with force magnitude

$$F_0 = \frac{3\mu_0 m^2}{4\pi\sigma^4} = \frac{\pi}{48}\mu_0 M_p^2\sigma^2. \tag{7}$$

This force magnitude can be turned into a reference stress, $\tau^* = F_0/\sigma^2$, which will be used to normalize shear stress.

The fluid interacts with particles via viscous drag, $F_i = -C_d(\dot{\mathbf{x}}_i - \mathbf{v}_c)$, where η_c is the carrier fluid viscosity, $\dot{\mathbf{x}}_i$ and $\mathbf{v}_c$ are the particle and carrier fluid velocity respectively, and C_d is the coefficient of drag, where for Stokes drag, $C_d = 3\pi\sigma\eta_c$. In most microscopic models, the carrier fluid moves independently of the particles, allowing us to assume a carrier fluid velocity profile. In shear, the bulk fluid, and thus the carrier fluid moves with velocity $\mathbf{v}_c = \dot{\gamma}y\mathbf{e}_x$, where y is the distance from the stationary surface.

Solving for the trajectory of the particle, the equations of motions for the particle are

$$m_i\ddot{\mathbf{x}}_i + C_d\dot{\mathbf{x}}_i - \sum_{j=1}^{N}\mathbf{F}_{ij}(\mathbf{x}_i, \mathbf{x}_j) = C_d\dot{\gamma}y_i\mathbf{e}_x, \tag{8}$$

where $\mathbf{x}_i$ is the position of the ith particle, and for this equation only, m_i is the mass. The particle mass is small, so that the force contributions from particle acceleration are also small and occur at such a short time scale that $m_i\ddot{\mathbf{x}}_i$ can be set to zero [4]. This allows the full equations of motion to be placed into a kinematic form, which when placed in a dimensionless form yields

$$\frac{C_d}{F_0}\dot{\mathbf{x}}_i = \sum_{j=1}^{N}\frac{\mathbf{F}_{ij}(\mathbf{x}_i, \mathbf{x}_j)}{F_0} + \mathrm{Mn}\frac{y_i}{\sigma}\mathbf{e}_x, \tag{9}$$

where Mn is the Mason number, and is the sole term governing the shear response of the particles in the fluid. The Mason number is the ratio of microscopic shear forces to microscopic magnetic forces, defined as

$$\mathrm{Mn} = \frac{C_d\sigma\dot{\gamma}}{F_0} = \frac{3\pi\eta_c\dot{\gamma}}{\tau^*} = 144\frac{\eta_c\dot{\gamma}}{\mu_0 M_p^2}. \tag{10}$$

Because Mason number governs shear behavior of the particle structures, it will govern the breaking and reforming of the chains in the fluid, and can be used to predict the shear response of the fluid.

When apparent viscosity, $\tau/\dot{\gamma}$, is plotted against Mason number for experimental data, the apparent viscosity curves collapse to a single master curve, so that apparent viscosity is solely a function of Mason number. Thus, the Mason number acts as a non-dimensionalized input condition that yields one output condition, and it is through this result that we intend to relate the Bingham and Mason numbers. This nondimensionalization of experimental data allows low shear rate experimental data to be extrapolated to high shear rates, and will be used in our relationship between Bingham number and Mason number. In particular, this is useful as shear rates in practical MR devices can exceed $\dot{\gamma} > 10\,000\ \mathrm{s}^{-1}$, while rheometer experiments typically operate at $\dot{\gamma} < 1000\ \mathrm{s}^{-1}$.

The Mason number is often defined using the H field, where $M = 3\beta H$ with $\beta = (\mu_p - \mu_c)/(\mu_p + 2\mu_c)$ from the textbook problem of an isolated, linearly susceptible sphere in a uniform applied field, yielding

$$\mathrm{Mn}(H) = \frac{16\ \eta_c\dot{\gamma}}{\mu_0\mu_c\beta^2H^2}, \tag{11}$$

where μ_p and μ_c are the relative permeability of the particle and carrier fluid respectively. The H-based form has several benefits, among which are its amenability to theoretical analysis, applicability to inverse ferrofluids, and its ease of relation to the electric analogue used in electrorheological fluid analysis. While M is a derived quantity, experimentally, the magnetization curves of the fluid must always be known to determine the magnetic field within the testing device. The H-based analysis also requires measuring $\mu_p(H)$ for β, a process which involves measuring M. Using M or μ_p from a magnetometer invokes the assumption that the particle structure, and thus magnetization, is the same in both magnetometer and device, however in practice, this assumption appears successful [14]. Most importantly, Klingenberg showed that approaching saturation, the H based Mason number fails to deliver the desired coalescing of data onto a master curve [8]. In the context of device engineering, nonlinear magnetization must be accounted for, so that we choose to use a Mason number based on average particle magnetization. Also, because average particle magnetization is a measurable quantity, it can also be used to validate the assumed particle structure in models of MR fluids.

We also note that the Mason number definition sometimes varies in the literature. Here we define Mason number using a characteristic separation distance of a particle diameter, as it gives a useful definition of τ^*. This leads to a definition of Mn that is 32 times larger than that in [8].

3. Theory

We now seek to relate Mason number to Bingham number, so that microscopic results can be extended to macroscopic behavior, and vice versa. In order to relate Bingham number to Mason number, we observe that both are ratios of magnetic and viscous forces, at bulk and microscopic scales respectively. If we assume that the ratio of forces scales linearly from microscopic to bulk macroscopic properties, then Bingham (magnetic/viscous) and Mason (viscous/magnetic) numbers are inversely related. Assuming that the characteristic shear rate is the same in both Bi and Mn, solving for $\dot{\gamma}$ in (10) gives

$$\dot{\gamma} = \frac{F_0}{\sigma^2}\frac{1}{3\pi\eta_c}\mathrm{Mn} = \frac{\tau^*}{3\pi\eta_c}\mathrm{Mn}.$$

This can then be substituted into (5),

$$\mathrm{Bi} = 3\pi\frac{\tau_y/\tau^*}{\eta_{pl}/\eta_c}\mathrm{Mn}^{-1}, \tag{12}$$

giving us a relationship between Bingham and Mason number, in terms of two ratios. The first ratio, the ratio of the yield stress of the bulk material to the magnetic forces between two particles,

$$\frac{\tau_y}{\tau^*} = \frac{\tau_y}{\pi\mu_0 M_p^2/48} \tag{13}$$

is defined as the *normalized yield stress*. The second is the ratio of suspension viscosity to carrier fluid viscosity,

$$\frac{\eta_{pl}}{\eta_c} = \frac{\text{Suspension Viscosity}}{\text{Carrier Viscosity}}, \tag{14}$$

the *normalized viscosity*. Normalized yield stress, τ_y/τ^* represents how effective the magnetic attraction between particles manifests as a yield stress, and η_{pl}/η_c represents how the addition of particles

effects the suspension viscosity. Most importantly, we assert that these two ratios are constant fluid properties of fundamental interest, as will be shown below, and these are ratios that can be predicted from existing literature and theory.

Again, note that the Bingham number is the ratio of magnetically induced shear stress to viscous shear stress, and that the Mason number is the ratio of viscous shear stress to magnetically induced interparticle stress. Another useful perspective is that the product of Bingham number and Mason number is a constant, or

$$\mathrm{Bi\ Mn} = 3\pi\frac{\tau_y/\tau^*}{\eta_{\mathrm{pl}}/\eta_c} \tag{15}$$

thereby evincing our earlier hypothesis. The term on the right, a constant, acts as a figure of merit of the fluid–particle recipe, representing the effect the addition of particles has on yield stress divided by the corresponding increase in viscosity. This term will be expanded upon further in Section 4.

3.1. Normalized yield stress

In order to argue that τ_y/τ^* is a fluid property, we need to show that yield stress scales roughly proportionally to average particle magnetization across field strength. For low volume fraction fluids, average particle magnetization as a yield stress scaling function has been shown to be a successful scaling law [15]. For the high volume fraction, high yield stress fluids of interest in controllable force applications, an estimate for τ_y/τ^* can be obtained using existing fits of B vs. H and τ_y vs. H for a range fluids, and then solving for τ_y/τ^*. Carlson [16] offers the empirical and widely used fits

$$\tau_y = 271.7C\phi^{1.524}\tanh(5.04\mu_0 H) \tag{16}$$

$$B = 1.91\phi^{1.133}\left[1 - \exp(-10.97\mu_0 H)\right] + \mu_0 H \tag{17}$$

designed to cover iron-based fluids, including those sold by Lord Corporation. In these equations, τ_{MR} is in kPa, H is in A/m and the parameter C is 1.0, 1.16 or 0.95 depending on whether the carrier fluid is hydrocarbon oil, water, or silicon oil respectively. Neglecting the effect of carrier fluid, we can substitute these equations into τ_y/τ^* and obtain

$$\frac{\tau_y}{\tau^*} = \frac{1.43\phi^{1.257}\tanh(5.04\mu_0 H)}{\left[1 - \exp(-10.97\mu_0 H)\right]^2}. \tag{18}$$

For fields above $H=100$ kA/M, this equation is largely constant, depending solely on fluid volume fraction and carrier fluid, as initially required. However in the limit of $H=0$, (18) yields $\tau_y/\tau^* = \infty$, as M drops off faster than yield stress, but an examination of Carlson's data shows that his yield stress model overestimates the experimentally measured yield stress at low field strengths, so this issue can be neglected. Observing that for $0.2 \le \phi \le 0.5$, τ_y/τ^* is within 15% of ϕ, this allows the construction of the rule of thumb, $\tau_y/\tau^* \approx \phi$.

Beyond developing experimental rules of thumb for yield stress, normalized yield stress also appears in most particle level modeling work, however, typically in the form of τ_y/H^2. Pen and paper models work by assuming a particle structure, allowing the particles to magnetically interact, deforming the structure under shear, and then computing the interparticle forces to find the shear stress. Computational models follow a similar structure, but with a dynamic structural deformation [4,17,18]. In order to resolve some of the nonlinear magnetization in the particles, some models allow regions of the particle to saturate, obtaining $\tau_y \propto \phi H^{3/2} M_s^{1/2}$, but these models fail near M_s [19,20]. The unsurprising solution is to work in terms of averaged particle magnetization, as it allows a model to work across the entire spectrum of applied field, as shown in [21]. The benefit of this nondimensional form for yield stress is that it takes τ_y, a field dependent term, and puts it in a form that is roughly independent of field, depends only on particle type and concentration, and can be predicted using various analytical methods.

3.2. Normalized viscosity

The normalized viscosity ratio, $\eta_{\mathrm{pl}}/\eta_c$, is the ratio of off-state viscosity to carrier viscosity. The typical assumptions about plastic viscosity are that it is independent of applied magnetic field, and can be determined by measurements of the fluid with no field applied. Since carrier fluid viscosity is independent of field, $\eta_{\mathrm{pl}}/\eta_c$ will be a function only of the addition of the particles, and thus a fundamental property of the fluid. Since the particles in an MR fluid are traditionally hard spheres, a prediction of this material property can be determined from the theoretical and empirical relations developed in the study of hard sphere dispersions [22], for example, the empirical Quemada relation,

$$\frac{\eta}{\eta_c} = \left(1 - \frac{\phi}{\phi_{max}}\right)^{-2} \tag{19}$$

where ϕ_{max} is the maximum particle volume fraction. However, these hard sphere equations must be used with caution, as practical MR fluids use additives which significantly affect the plastic viscosity, and so generalized forms with more parameters may be required. Once an appropriate viscosity relationship has been found, Eq. (12) can be expressed as a function solely dependent on ϕ. The notion that normalized viscosity is constant can also be used to show that the highly temperature dependent post yield performance of MR fluids is caused only by changes in the carrier fluid [23].

However, while the assumption that η_{pl} is constant is effective in the practical analysis of MR devices, this assumption often breaks down when examining the rheogram of practical MR fluids. The plastic viscosity for a particular value of field is determined, in practice, from the high shear rate asymptote of rheogram or shear stress vs. shear rate data as shown Fig. 1. These plastic viscosities for discrete values of magnetization, while reasonably similar in value, are not necessarily identical to the off-state viscosity, so that there exists varying levels of shear thinning. The theory of hard sphere dispersions tells us that viscosity is dependent on particle structure, so when field is applied and the particles form chains, the applicability of dispersion theory to determine η_{pl} is questionable. In an attempt to resolve this dilemma, Berli and de Vincente developed a structure based model for viscosity [24], and used it to model traditional MR fluids as well as inverse ferrofluids. Their analysis leads to low and high shear rate viscosity plateaus, which can be well represented for a typical MR fluid as a Casson plastic,

$$\tau^{1/2} = \tau_y^{1/2} + (\eta_\infty \dot{\gamma})^{1/2}. \tag{20}$$

This introduces a field dependent viscosity term that smooths the transition between pre- and post-yield behavior, improving the quality of the fit for some fluids, which typically tend be small particle (thermally influenceable) low yield stress fluids. However, for consistency with the device engineering literature and for ease of analysis, the widely accepted Bingham plastic constant (post-yield) viscosity approximation is sufficient for our purposes.

4. Experiment

The Bingham–Mason relationship can be measured directly by examining apparent viscosity. Apparent viscosity, $\eta_{app} = \tau/\dot{\gamma}$, is the viscosity of a Newtonian fluid that would give the measured stress at the current shear rate. For a Bingham plastic, where

$$\tau = \tau_y + \eta_{pl}\dot{\gamma} \tag{21}$$

the apparent viscosity is

$$\eta_{app} = \tau_y/\dot{\gamma} + \eta_{pl} \tag{22}$$

The high shear rate limit of apparent viscosity is denoted as η_∞, and for a Bingham plastic, $\eta_\infty = \eta_{pl}$. Apparent viscosity is often normalized by η_∞, which for a Bingham plastic yields

$$\frac{\eta_{app}}{\eta_\infty} = \frac{\eta_{pl}}{\eta_{pl}} + \frac{\tau_y}{\eta_{pl}\dot{\gamma}} = 1 + \mathrm{Bi}. \tag{23}$$

Thus a measurement of apparent viscosity leads directly to a measurement of Bingham number. For MR fluids, a well known result is that when apparent viscosity is plotted against Mason number, a set of curves of apparent viscosity coalesce to a single master curve [8,24]. Therefore, by using normalized apparent viscosity plotted against Mason number, we obtain a single curve that allows us to directly relate Bingham number to Mason number for a particular MR fluid being measured.

Fig. 3 shows a measurement of apparent viscosity using the commercially available Lord MRF-140CG fluid, demonstrating the collapse of apparent viscosity curves across Mason number. This 20 °C temperature controlled data set was collected using a custom-built high shear rate ($\dot{\gamma} < 10\,000\ \mathrm{s}^{-1}$) Searle cell magnetorheometer [25]. High shear rates are achieved by using a narrow ($d = 0.25$ mm) active gap, and the concentric cylinder geometry ensures a uniform shear rate. Using $\dot{\gamma} \gg 0$ avoids nonlinearities associated with near yield flow, and ensures that the data is well modeled as a Bingham plastic. In this experimental procedure, a servomotor rotates the inner cylinder using an ascending staircase velocity profile, while the outer cylinder is connected to a fixed base by a 0.706 N m angular load cell. The applied magnetic field was simulated via a 2D axisymmetric FEM analysis and validated using sensing coil measurements of flux density, and the fluid magnetization was calculated using the characterized field and manufacturer supplied $B-H$ data. Since the carrier fluid formulation for Lord fluids is proprietary, the carrier fluid was obtained by allowing a well mixed sample to separate, and then decanting the sediment-free upper layer. Carrier fluid viscosity was measured on an Anton Paar Phyisca MCR-300 rheometer, with the average of three runs to yield a viscosity value of $\eta_c = 9.9$ mPa s at 25 °C.

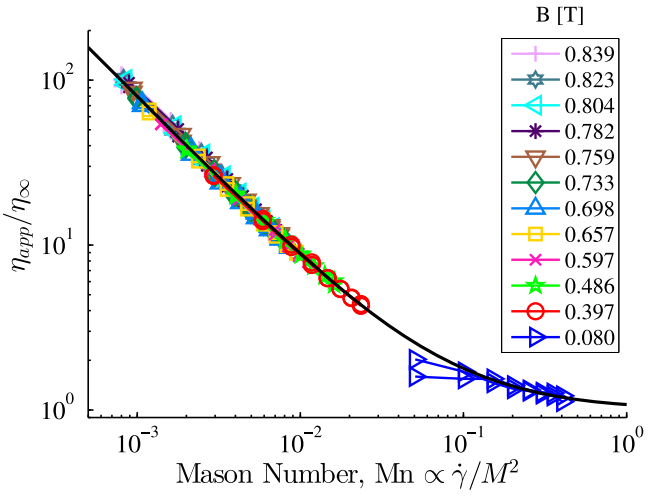

Fig. 3. Normalized apparent viscosity for Lord MRF-140CG.

For magnetorheological fluids, apparent viscosity is typically fitted to a curve of the form

$$\frac{\eta_{app}}{\eta_\infty} = 1 + K\mathrm{Mn}^{-1}, \tag{24}$$

where K is a fitted parameter. In Fig. 3, we show such a fit, with $K = 0.078$, and $\eta_\infty = 0.59$ Pa s. Since MR fluids are well described by the Bingham plastic model, from (23), $\eta_{app}/\eta_\infty = 1 + \mathrm{Bi}$, and from our experiment $\eta_{app}/\eta_\infty = 1 + K\mathrm{Mn}^{-1}$, then $\mathrm{Bi} \propto \mathrm{Mn}^{-1}$, validating (12).

The fitted parameter K is also known as the critical Mason number Mn^* [24,7,26], and corresponds to the Mason number where the low Mn asymptote of η_{app}/η_∞ intersects $\eta_{app}/\eta_\infty = 1$, or the Mason number where Bi = 1. From (12) the critical Mason number can be expressed as

$$\mathrm{Mn}^* = 3\pi\frac{\tau_y/\tau^*}{\eta_{pl}/\eta_c}, \tag{25}$$

which is also the product of Mason and Bingham numbers (15). The critical Mason number serves two purposes: it acts as a conversion factor between Mason number and Bingham number, and also acts as a fluid figure of merit. Critical Mason number converts a nondimensionalized input condition (Mason number) to nondimensionalized output condition (Bingham number), so that these two numbers can be easily related. Critical Mason number acts as a controllable force figure of merit with respect to the addition of particles, and can be thought of the benefit the addition of particles has had on yield stress to the penalty paid as in increase in viscosity. Fluids with a large Mn^* possess a larger controllable force ratio, while Mn^* decreases with increased volume fraction. Finally, because τ_y/τ^* and η_{pl}/η_c are analytically accessible ratios, we now have a way to determine critical Mason number during the fluid design process.

However, note that Eq. (24) is limited to fluids well described by the Bingham plastic model, a description not suited to all electrically and magnetically responsive fluids. In some of these fluids, the fluid scales between $\mathrm{Mn}^{-2/3}$ and Mn^{-1}, where fluids with particles influenced by thermal motion depart from Mn^{-1} scaling [27–30]. However these fluids are typically low yield stress fluids measured at low field strengths, and this is attributed to the effects of Brownian forces on the particle [31]. However, in the context of controllable force applications, where high yield stress fluids are used, thermal effects on the particles are relatively small, and the Bingham plastic model and Mn^{-1} scaling are a proven success [8]. These effects manifest at high Mn, with experimental apparent viscosity data decreasing slower than (24) predicts. However for the purpose of relating Bi and Mn, typically at that point Bi is small (Bi < 2), and thus negligible for controllable force applications. Such errors can potentially be resolved through the use of Casson plastic type models [24].

Finally, it should be noted that fitting a line to the apparent viscosity curve can be problematic, especially when high Mn data is unavailable, as there is no clear value for η_∞. An alternate approach is to plot normalized stress, τ/τ^* against Mason number, shown in Fig. 4. The normalized stress plot demonstrates, like the apparent viscosity plot, that stress values can be collapsed across varying field strengths through Mason number based analysis, while retaining plastic viscosity information at low Mason numbers, unlike apparent viscosity, offering an alternate, improved master curve. This makes determining τ_y/τ^* and η_{pl}/η_c much easier,

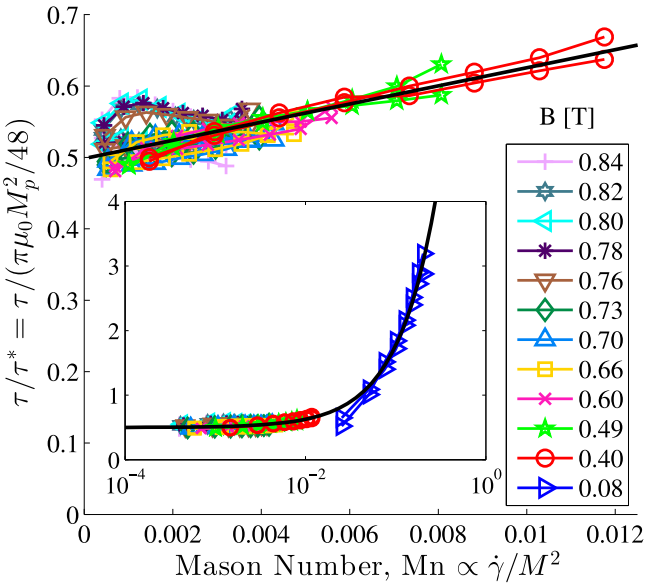

Fig. 4. Normalized stress vs. Mason number, with high Mason number data as inset. The black line corresponds to a linear least squares fit, and shows how the low Mason based fit agrees with the inset high Mason number data.

as for a Bingham plastic, normalized stress is given by

$$\frac{\tau}{\tau^*} = \frac{\tau_y}{\tau^*} + \frac{\eta_{pl}/\eta_c}{3\pi}\mathrm{Mn}. \tag{26}$$

Then a simple linear least-squares fit gives $\tau_y/\tau^* = 0.499$ and $\eta_{pl}/\eta_c = 59.9$, from which we generated the previously stated values for K and η_∞. This procedure has the benefit that it separates τ_y/τ^* and η_{pl}/η_c, allowing them to be fit separately, instead of confounding the two terms into K. This fitting procedure works even when there is no high Mason number data, as shown in Fig. 4. The benefits of plotting in this form are that it clearly shows the successful normalization of yield stress, as well as that η_{pl}/η_c is independent of field, and separates them into discrete elements for easy linear fitting, and serves as a complement to typical stress–shear rate graphs and normalized apparent viscosity graphs. The downside of this plot is that since it is no longer log–log, it much more clearly shows errors and noise in experimental data, and can be quite sensitive to errors in characterization of the magnetic field.

5. Discussion

The primary purpose of our analysis is to develop a non-dimensional scaling relationship to be used to relate the performance of different devices. In traditional device design, several output parameters (τ_y, η_{pl} and Bi) must be accounted for across a large input space (magnetic field strength, shear rate and temperature), requiring extensive experimental characterization. We want to avoid this, and here Mason number analysis shines – it allows the performance of MR fluid data to be reduced to one single master curve, dependent solely on Mason number. Then to obtain the desired output quantity of controllable force, Eq. (12), yields the Bingham number. We also show that τ_y can be made independent of magnetization as τ_y/τ^*, and plastic viscosity can be temperature independent in the form of η_{pl}/η_c. This non-dimensionalization allows us to take low shear rate, low field data measured on a small fluid sample, and extend it to a large scale energy absorbing device with high fields and high shear rates with a high level of confidence. This is demonstrated for a large scale energy absorbing device operating at $\dot{\gamma} > 25\,000\ \mathrm{s}^{-1}$ in [32].

For pen and paper analysis, there exists the notion of a Mason number above which no chains can form in the fluid, posing an upper limit on the existence of the MR effect. However, if this limiting Mason number occurs at a low Bingham number, the loss in yield stress will not be an issue for experimental devices. In [33,34], the limiting Mason number was found to be $\mathrm{Mn} \approx 1$. Using (12), we can use our previously determined values of τ_y/τ^* and η_{pl}/η_c to find that at $\mathrm{Mn} = 1$, $\mathrm{Bi} = 0.08$, which indicates that this effect occurs at such low controllable force levels that it will have an insignificant effect on MR device performance.

The relation between Bingham and Mason number can also be used to inform the MR fluid design process. For example, let us assume that we have a damper with a given device geometry, and we seek to design a fluid such that the damper has a high maximum damping force at maximum field (τ_y/τ^*), a large Bingham number (Mn^*), and a sufficient sedimentation time [35]. For maximizing τ_y/τ^*, we can seek to increase yield stress by increasing M or by raising τ_y/τ^* itself. To increase M, one option is to use particles made out of novel, highly magnetic materials, or alternatively to replace the carrier fluid with ferrofluids, with the intention of increasing the particle magnetization [36,37]. To raise τ_y/τ^*, we can either increase volume fraction, or more interestingly, use novel particle formulations, such as fluids with nanowires, nonmagnetic particles or differently shaped particles [38–42]. Once the particle geometry and type are chosen, choosing the volume fraction is a matter of managing the trade off between yield stress and viscosity, as raising volume fraction raises η_{pl}/η_c faster than τ_y/τ^*, reducing Mn^*. So if we seek to maximize controllable force, the only remaining free variable in (12) is η_c in Mason number. The final constraint, settling time, is expected to be dependent on the carrier fluid viscosity and density, and particle geometry, so for our case of fixed particle formulation, long settling times (large η_c) must be balanced against large controllable force ratios (small η_c).

6. Conclusion

We demonstrated that $\mathrm{Bi} \propto \mathrm{Mn}^{-1}$, or $\mathrm{Bi} \times \mathrm{Mn}$ is a constant, in magnetorheological fluids, both theoretically and experimentally, resulting in Eq. (12), a simple algebraic relation. Theoretically, we demonstrated that this behavior arises because microscopic forces and macroscopic forces are linearly related, and experimentally validated this relationship through measurements of apparent viscosity on a high shear rate Searle cell-type rheometer. It was shown that that the relationship between Bingham number and Mason number depends on two nondimensional quantities, τ_y/τ^* and η_{pl}/η_c, and we demonstrated that these ratios represent fundamental fluid properties that are experimentally and analytically accessible. These ratios also define the critical Mason number, Mn^*, through Eq. (25). In order to identify these quantities, fluid stress measurements were placed in the form of τ/τ^* vs. Mn, allowing for easy identification of τ_y/τ^* and η_{pl}/η_c.

Finally, this relation was used to examine a Mason number corresponding to a theoretical upper limit on the performance of MR fluids, and showed that this Mason number corresponded to Bingham numbers outside the operational range for experimental results. Finally, the MR fluid design process was looked at through the lens of $\mathrm{Bi} \propto \mathrm{Mn}^{-1}$, showing how current approaches for novel fluids fall within the recommendations made by the analytical methods in this paper.

Acknowledgements

S.G. Sherman was supported by a National Science Foundation Graduate Research Fellowship under Grant no. DGE1322106 during the course of this research.

References

[1] Y.-T. Choi, N.M. Wereley, Biodynamic response mitigation to shock loads using magnetorheological helicopter crew seat suspensions, J. Aircr. 42 (5) (2005) 1288–1295, 10.2514/1.6839.

[2] N.M. Wereley, Y.-T. Choi, H.J. Singh, Adaptive energy absorbers for drop-induced shock mitigation, J. Intell. Mater. Syst. Struct. 22 (6) (2011) 515–519. http://dx.doi.org/10.1177/1045389X10393767, URL: ⟨http://jim.sagepub.com/cgi/doi/10.1177/1045389X10393767⟩.

[3] H.J. Singh, N.M. Wereley, Adaptive magnetorheological shock isolation mounts for drop-induced impacts, Smart Mater. Struct. 22 (12) (2013) 122001. http://dx.doi.org/10.1088/0964-1726/22/12/122001, URL: ⟨http://stacks.iop.org/0964-1726/22/i=12/a=122001?key=crossref.f87498cf631392274fc5895e9bc8e374⟩.

[4] D.J. Klingenberg, F. van Swol, C.F. Zukoski, Dynamic simulation of electrorheological suspensions, J. Chem. Phys. 91 (12) (1989) 7888. http://dx.doi.org/10.1063/1.457256, URL: ⟨http://link.aip.org/link/JCPSA6/v91/i12/p7888/s1&Agg=doi⟩.

[5] M. Mohebi, N. Jamasbi, J. Liu, Simulation of the formation of nonequilibrium structures in magnetorheological fluids subject to an external magnetic field, Phys. Rev. E 54 (5) (1996) 5407–5413. http://dx.doi.org/10.1103/PhysRevE.54.5407.

[6] K. Han, Y.T. Feng, D.R.J. Owen, Three-dimensional modelling and simulation of magnetorheological fluids, Int. J. Numer. Methods Eng. 84 (11) (2010) 1273–1302. http://dx.doi.org/10.1002/nme.2940, URL: ⟨http://doi.wiley.com/10.1002/nme.2940⟩.

[7] L. Marshall, C.F. Zukoski, J.W. Goodwin, Effects of electric fields on the rheology of non-aqueous concentrated suspensions, J. Chem. Soc., Faraday Trans. 185 (9) (1989) 2785. http://dx.doi.org/10.1039/f19898502785 ⟨http://xlink.rsc.org/?DOI=f19898502785⟩.

[8] D.J. Klingenberg, J.C. Ulicny, M.A. Golden, Mason numbers for magnetorheology, J. Rheol. 51 (5) (2007) 883. http://dx.doi.org/10.1122/1.2764089 ⟨http://link.aip.org/link/JORHD2/v51/i5/p883/s1&Agg=doi⟩.

[9] S. Melle, O. Calderón, M. Rubio, G. Fuller, Microstructure evolution in magnetorheological suspensions governed by Mason number, Phys. Rev. E 68 (4) (2003) 041503. http://dx.doi.org/10.1103/PhysRevE.68.041503, URL: ⟨http://link.aps.org/doi/10.1103/PhysRevE.68.041503⟩.

[10] R.S. Allan, S.G. Mason, Particle behaviour in shear and electric fields. I. Deformation and burst of fluid drops, Proc. R. Soc. A: Math., Phys. Eng. Sci. 267 (1328) (1962) 45–61. http://dx.doi.org/10.1098/rspa.1962.0082, URL: ⟨http://rspa.royalsocietypublishing.org/cgi/doi/10.1098/rspa.1962.0082⟩.

[11] G.M. Kamath, M.K. Hurt, N.M. Wereley, Analysis and testing of Bingham plastic behavior in semi-active electrorheological fluid dampers, Smart Mater. Struct. 5 (5) (1996) 576–590. http://dx.doi.org/10.1088/0964-1726/5/5/007, URL: ⟨http://stacks.iop.org/0964-1726/5/i=5/a=007?key=crossref.a3d91bf4e5710a7d9709780fd511e695⟩.

[12] N.M. Wereley, L. Pang, Nondimensional analysis of semi-active electrorheological and magnetorheological dampers using approximate parallel plate models, Smart Mater. Struct. 7 (5) (1998) 732–743. http://dx.doi.org/10.1088/0964-1726/7/5/015, URL: ⟨http://stacks.iop.org/0964-1726/7/i=5/a=015?key=crossref.7a2bc9c96a9d2c2abb03481d6e6f4422⟩.

[13] N.M. Wereley, J.U. Cho, Y.T. Choi, S.B. Choi, Magnetorheological dampers in shear mode, Smart Mater. Struct. 17 (1) (2008) 015022. http://dx.doi.org/10.1088/0964-1726/17/01/015022 ⟨http://stacks.iop.org/0964-1726/17/i=1/a=015022?key=crossref.fda5df5108adfa52fb6037fdca94fdb6⟩.

[14] J. de Vicente, G. Bossis, S. Lacis, M. Guyot, Permeability measurements in cobalt ferrite and carbonyl iron powders and suspensions, J. Magn. Magn. Mater. 251 (1) (2002) 100–108. http://dx.doi.org/10.1016/S0304-8853(02)00484-5 ⟨http://linkinghub.elsevier.com/retrieve/pii/S0304885302004845⟩.

[15] F. Vereda, J. de Vicente, J.P. Segovia-Gutiérrez, R. Hidalgo-Alvarez, Average particle magnetization as an experimental scaling parameter for the yield stress of dilute magnetorheological fluids, J. Phys. D: Appl. Phys. 44 (42) (2011) 425002. http://dx.doi.org/10.1088/0022-3727/44/42/425002, URL: ⟨http://stacks.iop.org/0022-3727/44/i=42/a=425002?key=crossref.3856e3acaa76c7e4ec47b10bdfdedb9d⟩.

[16] J.D. Carlson, MR fluids and devices in the real world, Int. J. Mod. Phys. B 19 (7–9) (2005) 1463–1470. http://dx.doi.org/10.1142/S0217979205030451, URL: ⟨http://www.worldscinet.com/abstract?id=pii:S0217979205030451⟩.

[17] S.G. Sherman, N.M. Wereley, Effect of particle size distribution on chain structures in magnetorheological fluids, IEEE Trans. Magn. 49 (7) (2013) 3430–3433. http://dx.doi.org/10.1109/TMAG.2013.2245409, URL: ⟨http://ieeexplore.ieee.org/lpdocs/epic03/wrapper.htm?arnumber=6559074⟩.

[18] D.J. Klingenberg, C.H. Olk, M.A. Golden, J.C. Ulicny, Effects of nonmagnetic interparticle forces on magnetorheological fluids, J. Phys. Condens. Matter 22 (32) (2010) 324101–324105. http://dx.doi.org/10.1088/0953-8984/22/32/324101, URL: ⟨http://www.ncbi.nlm.nih.gov/pubmed/21386477⟩.

[19] J. Ginder, L. Davis, L. Elie, Rheology of magnetorheological fluids: models and measurements, Int. J. Mod. Phys. B 10 (23n24) (1996) 3293–3303. http://dx.doi.org/10.1142/S0217979296001744, URL: ⟨http://www.worldscientific.com/doi/abs/10.1142/S0217979296001744⟩.

[20] G. Bossis, S. Lacis, A. Meunier, O. Volkova, Magnetorheological fluids, J. Magn. Magn. Mater. 252 (2002) 224–228. http://dx.doi.org/10.1016/S0304-8853(02)00680-7, URL: ⟨http://linkinghub.elsevier.com/retrieve/pii/S0304885302006807⟩.

[21] M.R. Jolly, J.D. Carlson, B.C. Muñoz, A model of the behaviour of magnetorheological materials, Smart Mater. Struct. 5 (5) (1996) 607–614. http://dx.doi.org/10.1088/0964-1726/5/5/009, URL: ⟨http://stacks.iop.org/0964-1726/5/i=5/a=009?key=crossref.9f2d9deaecbd39fb857ce036d69a6ab1⟩.

[22] J. Mewis, N.J. Wagner, Colloidal Suspension Rheology, Cambridge University Press, Cambridge, 2012.

[23] S.G. Sherman, L.A. Powell, N.M. Wereley, Scaling temperature dependent rheology of magnetorheological fluids, J. Appl. Phys. 2015, in press.

[24] C.L.A. Berli, J. de Vicente, A structural viscosity model for magnetorheology, Appl. Phys. Lett. 101 (2) (2012) 021903. http://dx.doi.org/10.1063/1.4734504, URL: ⟨http://link.aip.org/link/APPLAB/v101/i2/p021903/s1&Agg=doi⟩.

[25] A.C. Becnel, W. Hu, N.M. Wereley, Measurement of magnetorheological fluid properties at shear Rates of up to 25 000 s, IEEE Trans. Magn. 48 (11) (2012) 3525–3528. http://dx.doi.org/10.1109/TMAG.2012.2207707, URL: ⟨http://ieeexplore.ieee.org/lpdocs/epic03/wrapper.htm?arnumber=6332988⟩.

[26] J. de Vicente, D.J. Klingenberg, R. Hidalgo-Alvarez, Magnetorheological fluids: a review, Soft Matter 7 (8) (2011) 3701. http://dx.doi.org/10.1039/c0sm01221a, URL: ⟨http://xlink.rsc.org/?DOI=c0sm01221a⟩.

[27] T. Halsey, J. Martin, D. Adolf, Rheology of electrorheological fluids, Phys. Rev. Lett. 68 (10) (1992) 1519–1522. http://dx.doi.org/10.1103/PhysRevLett.68.1519, URL: ⟨http://link.aps.org/doi/10.1103/PhysRevLett.68.1519⟩.

[28] E. Lemaire, A. Meunier, G. Bossis, J. Liu, D. Felt, P. Bashtovoi, N. Matoussevitch, Influence of the particle size on the rheology of magnetorheological fluids, J. Rheol. 39 (5) (1995) 1011. http://dx.doi.org/10.1122/1.550614, URL: ⟨http://link.aip.org/link/?JOR/39/1011/1&Agg=doi⟩.

[29] B.J. de Gans, N.J. Duin, D. van den Ende, J. Mellema, The influence of particle size on the magnetorheological properties of an inverse ferrofluid, J. Chem. Phys. 113 (5) (2000) 2032. http://dx.doi.org/10.1063/1.482011, URL: ⟨http://scitation.aip.org/content/aip/journal/jcp/113/5/10.1063/1.482011⟩.

[30] O. Volkova, G. Bossis, M. Guyot, V. Bashtovoi, A. Reks, Magnetorheology of magnetic holes compared to magnetic particles, J. Rheol. 44 (1) (2000) 91. http://dx.doi.org/10.1122/1.551075, URL: ⟨http://link.aip.org/link/JORHD2/v44/i1/p91/s1&Agg=doi⟩.

[31] G. Bossis, O. Volkova, S. Lacis, A. Meunier, Magnetorheology: fluids, structures and rheology, in: S. Odenbach (Ed.), Ferrofluids, Lecture Notes in Physics, vol. 594, Springer, Berlin, Heidelberg, 2002, pp. 202–230. http://dx.doi.org/10.1007/3-540-45646-5, URL: ⟨http://link.springer.com/10.1007/3-540-45646-5⟩.

[32] A.C. Becnel, S. Sherman, W. Hu, N.M. Wereley, Nondimensional scaling of magnetorheological rotary shear mode devices using the Mason number, J. Magn. Magn. Mater. (2014), in press, http://dx.doi.org/10.1016/j.jmmm.2014.10.049.

[33] S.G. Sherman, N.M. Wereley, Performance of magnetorheological fluids beyond the chain based shear limit, J. Appl. Phys. 115 (17) (2014) 17B523. http://dx.doi.org/10.1063/1.4867963, URL: ⟨http://scitation.aip.org/content/aip/journal/jap/115/17/10.1063/1.4867963⟩.

[34] J.E. Martin, R.A. Anderson, Chain model of electrorheology, J. Chem. Phys. 104 (12) (1996) 4814. http://dx.doi.org/10.1063/1.471176, URL: ⟨http://link.aip.org/link/JCPSA6/v104/i12/p4814/s1&Agg=doi⟩.

[35] J.D. Carlson, What makes a good MR fluid? J. Intell. Mater. Syst. Struct. 13 (7–8) (2002) 431–435. http://dx.doi.org/10.1106/104538902028221, URL: ⟨http://jim.sagepub.com/cgi/doi/10.1106/104538902028221⟩.

[36] J.D. Carlson, K.D. Weiss, Magnetorheological Materials based on Alloy Particles, U.S. Patent No. 5382373, 1995.

[37] J.M. Ginder, L.D. Elie, L.C. Davis, Magnetic fluid-based magnetorheological fluids, U.S. Patent No. 5549837, 1996.

[38] D.T. Zimmerman, R.C. Bell, J.A. Filer, J.O. Karli, N.M. Wereley, Elastic percolation transition in nanowire-based magnetorheological fluids, Appl. Phys. Lett. 95 (1) (2009) 014102. http://dx.doi.org/10.1063/1.3167815, URL: ⟨http://link.aip.org/link/APPLAB/v95/i1/p014102/s1&Agg=doi⟩.

[39] G.T. Ngatu, N.M. Wereley, J.O. Karli, R.C. Bell, Dimorphic magnetorheological fluids: exploiting partial substitution of microspheres by nanowires, Smart Mater. Struct. 17 (4) (2008) 045022. http://dx.doi.org/10.1088/0964-1726/17/4/045022, URL: ⟨http://stacks.iop.org/0964-1726/17/i=4/a=045022?key=crossref.bf5cd336229d731058f3a07ce62ea5dd⟩.

[40] L.A. Powell, N.M. Wereley, J. Ulicny, Magnetorheological fluids employing substitution of nonmagnetic for magnetic particles to increase yield stress, IEEE Trans. Magn. 48 (11) (2012) 3764–3767. http://dx.doi.org/10.1109/TMAG.2012.2202885 ⟨http://ieeexplore.ieee.org/lpdocs/epic03/wrapper.htm?arnumber=6332987⟩.

[41] K. Shah, D. Xuan Phu, S.B. Choi, Rheological properties of bi-dispersed magnetorheological fluids based on plate-like iron particles with application to a small-sized damper, J. Appl. Phys. 115 (20) (2014) 203907. http://dx.doi.org/10.1063/1.4879681.

[42] J. de Vicente, J.P. Segovia-Gutiérrez, E. Andablo-Reyes, F. Vereda, R. Hidalgo-Alvarez, Dynamic rheology of sphere- and rod-based magnetorheological fluids, J. Chem. Phys. 131 (19) (2009) 194902. http://dx.doi.org/10.1063/1.3259358, URL: ⟨http://www.ncbi.nlm.nih.gov/pubmed/19929071⟩.